$TiO_2/Bi_2S_3/Cu$ as a working electrode in Quantum Dots Sensitized Solar Cells

A Project Report Submitted

As part of the requirements for the degree of

MASTER OF SCIENCE

By

DEEPAK

(Roll No. CY14MSCST11004)

Under the supervision of

Dr. Ch. Subrahmanyam

भारतीय प्रौद्योगिकी संस्थान हैदराबाद
Indian Institute of Technology Hyderabad

to the

DEPARTMENT OF CHEMISTRY

INDIAN INSTITUTE OF TECHNOLOGY HYDERABAD
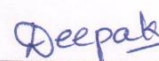
INDIA

APRIL, 2016

Declaration

I hereby declare that the matter embodied in this report is the result of investigation carried out by me in the Department of Chemistry, Indian Institute of Technology Hyderabad under the supervision of **Dr. Ch. Subrahmanyam**.
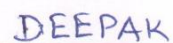
In keeping with general practice of reporting scientific observations, due to acknowledgement has been made wherever the work described is based on the findings of other investigators.

Signature of the Supervisor

Deepak

(Signature)

DEEPAK

(Student Name)

CY14MSCST11004

(Roll No)

Approval Sheet

This thesis of the project entitled "$TiO_2/Bi_2S_3/Cu$ as a working electrode in Quantum Dots Sensitized Solar Cells" by Deepak (CY14MSCST11004) is approved for the award of the degree of **Master of Science** in **Chemistry** from **Indian Institute of Technology Hyderabad** during the year 2015-2016.
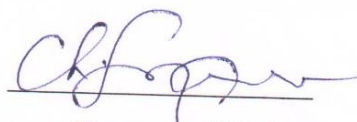
Dr. SURENDRA K. MARTHA
Assistant Professor
Department of Chemistry
Indian Institute of Technology Hyderabad

-Name and affiliation-

Examiner

-Name and affiliation-

Examiner

-Name and affiliation-

Adviser

-Name and affiliation-

Chairman

(iii)

<u>Acknowledgement</u>

I Deepak, express my gratitude to **Dr.Ch. Subrahmanyam** sir, who has through his vast experience and knowledge has been able to guide me successfully towards the completion of the project.

I also take this opportunity to thanks Departmental Head **Dr. Melepurath Deepa.**

I would hereby, make most of the opportunity by expressing my sincerest thank to **Mr. Palyam Subramanyam** for his continuous support, inspiration and guidance. Whose teaching gave me conceptual understanding and clarity of comprehension, which ultimately made my job much easier.

I am grateful to all my lab mates **Mr. Debjyoti Ray, Miss L Chandana, Mr. V Ashok Kumar, Mr. Bhairi Lakshminarayana, Mr. Krushnamurty Killi** for their cooperation and help.

 Credit also goes to all my friends whose encouragement kept me in good stead. Their continuous support has given me the strength and confidence to complete the project without any difficulty. I also thank to IIT Hyderabad for providing me the best facilities and equipment's to work. I am grateful to all the faculty members in the department of chemistry at IIT Hyderabad for their guidance.

Dedicated to

My Parents

Abstract

Bi_2S_3 is a promising material for Quantum Dot sensitized solar cells (QDSSCs). Probably the major reasons are: its low toxicity, low cost and its high absorption coefficient. The band gap of bulk Bi_2S_3 material is 1.3eV but in Quantum Dots (QDs) it varies from 1.3 to 1.7eV. In present work, we are reporting Bi_2S_3 QDs Sensitized over mesoporous oxide (TiO_2) and application of copper Nanoparticles (NPs) fabrication on TiO_2/Bi_2S_3 devices. The deposition of Bi_2S_3 QDs on TiO_2 was done by Successive Ionic Layer Adsorption and Reaction (SILAR) and fabrication of Cu NPs on TiO_2/Bi_2S_3 by electrophoretic deposition method. Finally, the maximum power conversion efficiency (PCE) is 3.90 % for $TiO_2/Bi_2S_3/Cu$ with functionalized multi walled carbon nanotubes (MWCNTs) as a counter electrode.

Abbreviations:

QDSSCs - Quantum Dot sensitized solar cells.

QDs - Quantum Dots

NPs - Nanoparticles

Bi_2S_3 - Bismuth Sulphide

TiO_2 - Titanium dioxide

PCE - Power Conversion Efficiency

MWCNTs - Multi Walled Carbon Nanotubes

PV – Photovoltaic

CdTe - Cadmium Telluride

eV – Electron Volt.

CIGS- Copper Indium Gallium Selenide.

MEG - Multiple Exciton Generation.

ZnO – Zinc Oxide

V_{oc} – Open Circuit Voltage

I_{sc} – Short Circuit Current

FF – Fill Factor

IPCE – Incident Photon to Carrier Efficiency

FTO - Fluorine doped Tin Oxide

XRD – X-Rays Diffraction

CV – Cyclic Voltammetry

ITO – Indium Tin Oxide

UV – Ultra Violet

EPD - Electrophoretic Deposition

DC – Direct Current

EIS - Electrochemical Impedance Spectroscopy

SEM – Scanning Electron Microscopy

LSPR – Localized Surface Plasmon Resonance

SPR - Surface Plasmon Resonance

VB – Valance Band

CB – Conduction Band

List of tables: Page No.

List of Figures Page No.

(ix)

Contents

Chapter 3

Result and discussion

Chapter 1

Introduction

1.1 Background:

The photovoltaic effect was first observed by Alexandre-Edmond Becquerel in 1839. [1] The first p-n junction solar cell came in knowledge by RCA and the Bell labs with an efficiency of 6% (In 1954). [2][3] Until late 1980s, the development was on silicon based solar cells. Even today silicon based solar cells are popular due to a high efficiency-to-cost ratio, the absence of environmental degradation issues, and great reliability. [4] First-generation solar cells based on crystalline silicon are already commercialized, and associated with high efficiencies of 15−20%. But due to tedious manufacturing processes and high producing cost, researchers focused on alternatives to silicon solar cells, which led to the discovery of second generation solar cells, known as amorphous or polycrystalline thin-film solar cells e.g. CdTe and CIGS thin-film cells. [5] Third generation of PV has vision of high efficiency and also low production cost. Dye-sensitized solar cells and organic solar cells and QDSSCs are typical examples of 3rd generation solar cells. Dye-sensitized solar cells have reported a high efficiency of more than 12 %[6] In the case of organic solar cells, the recently reported efficiency is 10.3%.[7] First QDs-sensitized solar cell was reported in 1998.[8] Now a days the efficiency of QDs-sensitized solar cells is above 8%.[9]

1.2 Motivation on QDs-sensitized Solar cells research:

In case of QDs-sensitized solar cells we are using QDs as sensitizer and due to tunability of their band gap they are very useful in PV cells. Quantum dots are semiconducting nanoparticles that are able to confine excitons in three dimensions. The advantages of using QDs are many fold, namely,

- Band gap tunability
- Large extinction coefficient
- Higher stability towards oxygen and water.
- Multiple electron-hole pair generation
- Low cost

1.2.1 Band gap tunability:

Quantum dots are nano particles or nanocrystals of a semiconducting material with diameters in the range of 2-10 nm (mostly). In QDs, electrons and holes are confined in three dimensions. Photons with energies below the semiconductor band gap are not absorbed. QDs absorbs the photons which are of same energy or higher in energy as of band gap energy. The

1

most important property of semiconductor nanocrystals is that optical density is function of size of NPs. Fig.1 shows as the size reduced the electronic excitations move towards higher energy.
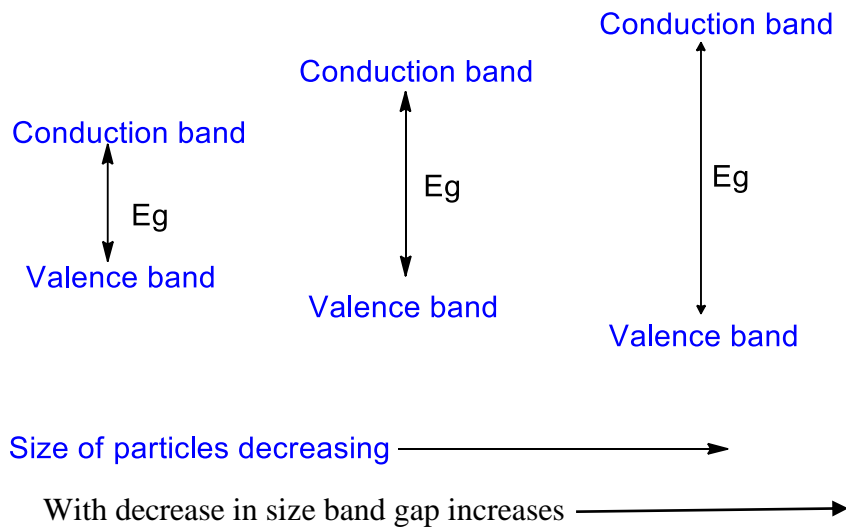
Fig. 1 Quantum confinement effect i.e. the effect of size on band gap.

This is due to quantum confinement, which occurs when nanocrystal radius being smaller than the exciton Bohr radius. The Bohr exciton radius is the average distance of electron and hole when an excitons are created in the bulk semiconductor. Electronic energy levels are not continuous in QDs as in the bulk, but are discrete due to confinement in physical dimensions of the electronic wave function. For, e.g. CdSe can be tuned from 1.7eV (deep red) to 2.4eV (green) by varying size 200 to $20A^o$. [10]

Varying the size of PbSe from bulk (which have band gap 0.28eV) to PbSe nanowires of size range 26.4 to 5.6 nm NWs can be tuned from 0.3eV to 0.6eV. [11] So, by changing size of particles the band gap of QDs also vary and absorb different wavelength of light which can ultimately change the color of QDs. Also previously reported [12] size dependent property includes the extinction coefficient.

1.2.2 Multiple exciton generation (MEG):

On shining QDs with the radiation of wavelength equal to band gap generates one pair of electron and hole. When the energy is higher than of the band gap, the electron and hole pair will be generated with excess kinetic energy. So, when absorbed photon have energy at least twice of the band gap then due to that excess energy another electron and hole pair can be generated shown in Fig.2. So, due to MEG effect, more than one electron and hole pair from absorption of one photon. [13]
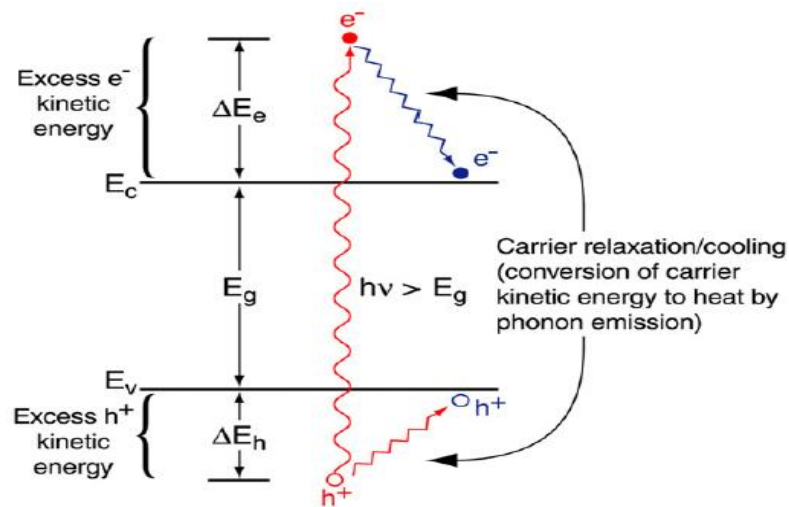
Fig. 2 Multiple excitation generation effect. [14]

1.3 Bi_2S_3 is promising material for future solar cells:

QDs can be made by different materials and QDSSCs are promising devices for power production in the future. Now a days researchers are keen to increase efficiency and want to prepare devices of low cost. Today lot of devices are formed based on quantum dot sensitization and among them CdS, CdTe, PbS, PbSe, and CdSe are common due to their optoelectronic properties. As Cd and Pb shows metal toxicity and we want to go towards environment friendly devices so, we can say that stabilization of Bi_2S_3 as a good material for PV is going away from metal toxicity.

- Bi_2S_3 band gap is 1.3eV- 1.7eV so it absorbs visible and Near IR part of solar spectrum.
- Bi_2S_3 shows high absorption coefficient. [15.]
- Also Bi_2S_3 is low cost material.

1.4 Effects of metal nanoparticle:

Metal nanoparticles are playing an important role in PV cells to improve the efficiency as well as from cost point of view. Metal NPs and QDs lead to increase photovoltaic behavior.

Fig. 3 Oscillation of electron cloud [16.]

Metal NPs enhance the PV characteristic due to:

- Large specific area means after metal NPs sensitization device shows large absorption
- Fermi level equilibrium
- Localized surface plasmon resonance(LSPR)

Localized surface plasmon resonance (LSPR) is oscillation of conduction band electrons when metal NPs interact with the electromagnetic field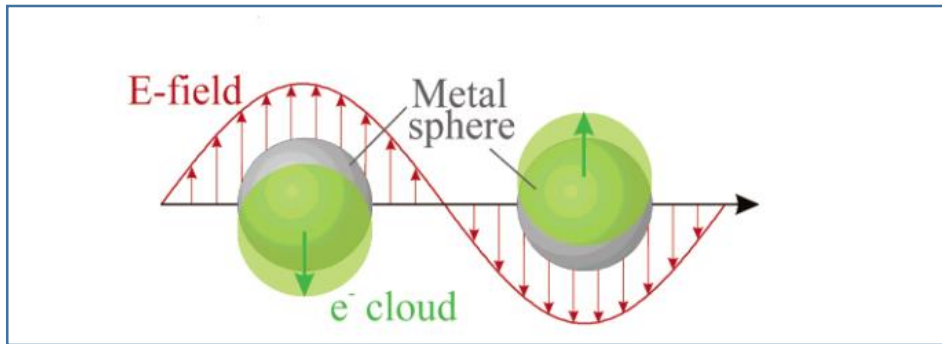 induced with light of smaller wavelength than that of size of metal NPs. Due to oscillating electric field the electrons of conduction band oscillate coherently because of restoring force arises from coulombic attraction between opposite charges (electrons and nuclei) gives oscillation of electron cloud are shown in Fig. 3 [16.] LSPR effect mostly shown by Au, Ag, and Cu NPs.

1.4.1 **Effect of metal NPs on optical absorption:**

The improvement of PCE is expected when metal NPs are in close neighbourhood to QD supported TiO_2. This is due to larger specific surface area, [17.] multiple scattering effects and improvement in oxidation and reduction of electrolyte due to their porous nature of the electrodes.

1.4.2 **Fermi level equilibrium between shell-core:**

When a semiconductor is illuminated radiations which are energetically equal to the band gap or higher energy then it gets excitation and electron and hole pairs are generated. When metal nanoparticles are in contact with excited QDs, due to electron transfer between shell and core Fermi levels of both equilibrate. The Plasmon absorption of gold shows blue shift due to presence of high energy resonance. [18.] Fermi level shift in case of copper NPs is reported by

authors when copper NPs are brought in contact with CdS QDs which are sensitized over TiO_2 i.e. TiO_2/CdS/Cu, as shown in Fig.4.[19.]
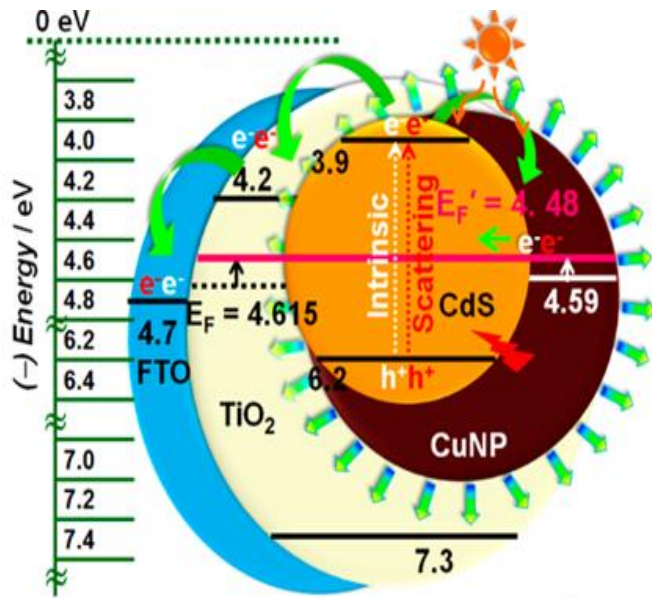

Fig. 4   Fermi level shift Cu NPs are in contact with CdS. [19.]

1.5 Fabrication Methods of Quantum Dots:

Fig. 5 shows the most common fabrication methods of Quantum dots over mesoporous photocatalysts.
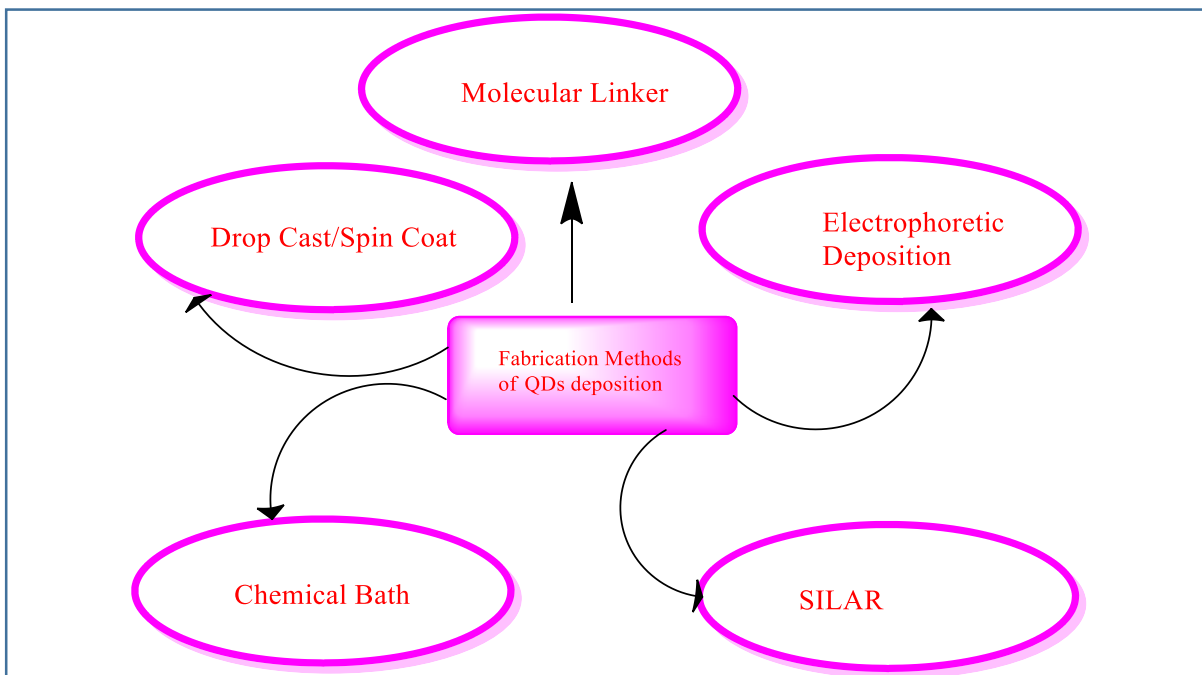

Fig. 5 Quantum dots deposition methods

Performance of device depends on method of preparation that alters surface area, morphology, optical properties. Also we know that with size of QDs, the positions of conduction band and valance band varies, which reflects in the performance of the device.

1.5.1 Successive Ionic Layer Adsorption and Reaction (SILAR):

In this method both cationic and anionic precursors are separately held, to deposit directly on the electrode surface. First electrode is immersed in cationic precursor and rinsed with solvent for removing unabsorbed salts and dried in an oven. After that the electrode is immersed in anionic precursor followed by washing with solvent, dried in oven. This is completion of one cycle and now with repetition of this process we can form number of cycles as the requirements of experiment. SILAR process have its own advantages like less expensive method and QDs deposition occurs on larger surface area than that of other deposition techniques. That's why it is very popular method to deposit QDs on desired surface. Fig. 6 shows deposition of QDs on mesoporous TiO_2 by SILAR method.
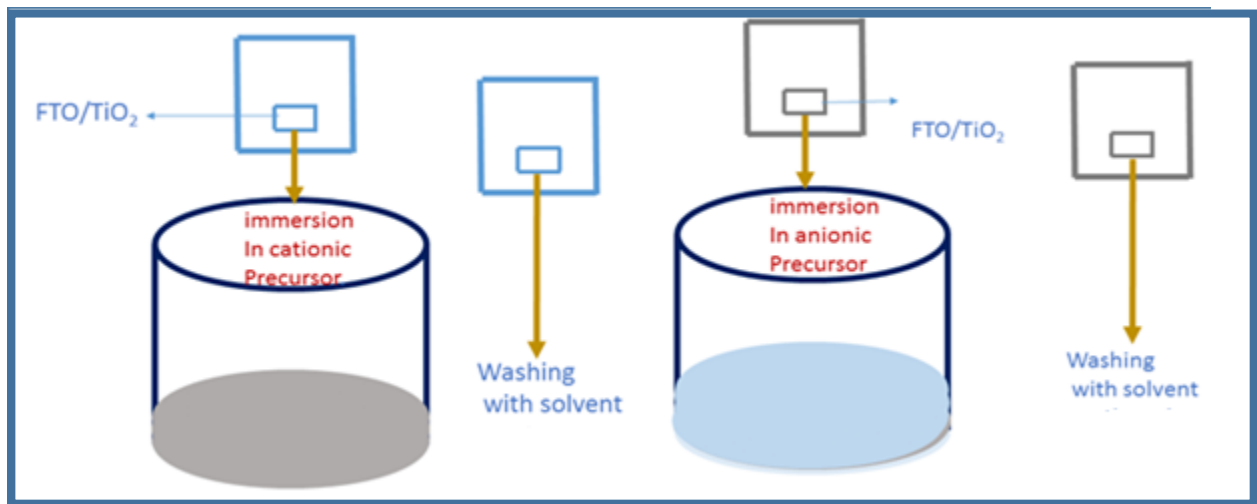
Fig. 6 SILAR deposition method of quantum dots.

1.5.2 Electrophoretic Deposition Method:

This method is used when QDs are pre-synthesized. In this method QDs are sensitized over electrode surface by applying DC electric field and already synthesized QDs suspension is present in between two electrodes [Fig. 7].
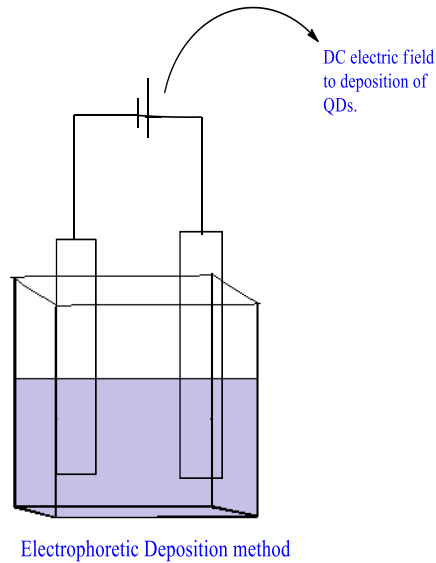
Fig. 7 Electrophoretic deposition method

1.6 Fundamental Parameters to study cell:

After designing solar cells we have to study its properties and concepts on which that is working so, according to concept there are lots of characterizations but J-V, plot is most fundamental parameter to study a solar cell.

1.6.1 J-V Plot:

J-V plot [fig.8] of solar cell is obtained by measuring the values of produced current with different applied potential. J-V curve is useful to check how ideal the device, which is under observation. J-V curve is the most fundamental characteristic in sense to the performance of the device i.e. it gives the address of V_{oc}, I_{sc}, FF and η. Open Circuit Voltage (V_{oc}) is the maximum voltage of solar cell which occurs at zero current and Short circuit current (I_{sc}) is the current obtained at zero voltage.
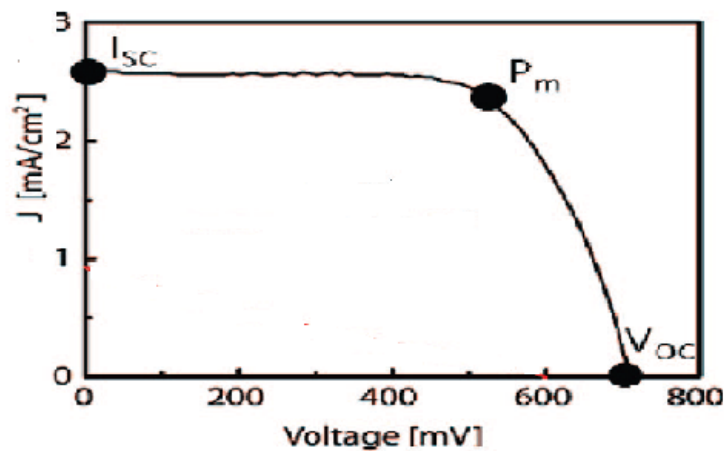
Fig. 8 J-V Plot for a solar cell [20.]

7

1.6.2 Fill Factor (FF):

Fill factor is area under the I-V curve and it is defined as:

$$FF = \frac{P_m}{I_{sc} \times V_{oc}}$$

$$P_m = I_{sc} \times V_{oc} \times FF$$

V_{oc} is Open Circuit Voltage

I_{sc} is Short circuit current

1.6.3 Power Conversion Efficiency (PCE) [η]:

Solar cell is conversion of solar energy to electric current i.e. conversion of photon energy to electricity. PCE is relation between input photon power and output electrical power.

$$\eta = \frac{P_m}{I \times A} \times 100\%$$

I is 100mW/cm^2 with standard one sun condition and A is area of cross-section of device

1.6.4 Incident-photon-to-carrier-efficiency (IPCE):

IPCE is another parameter which defines the performance of solar cell, it is photocurrent produced by cell at different wavelengths where excitations occur in semiconductor.

$$IPCE(\lambda) = \frac{1240 \times I_{sc}(\lambda)}{\lambda \times I(\lambda)} \times 100\%$$

$I_{sc}(\lambda)$ is J_{sc} in A/cm^2 and observed at different wavelengths.

$I(\lambda)$ is incident light density in W/cm^2 it is also wavelength dependent.

λ is excitation wavelength in nm.

1.7 Working principle of QDSSCs:

Solar cell is a device which converts photonic energy to electrical energy. In QDSSCs, QDs are fabricated on TiO_2 or ZnO mesoporous photocatalyst because once electrons are injected into the conduction band then they transfer it to collecting electrode surface. TiO_2 and ZnO have large band gap so they are transparent in visible region of sunlight. In QDSSCs we are using QDs as sensitizer which have narrow band gap and absorbs light in visible region or near IR region. Fig.9 shows the working principle of QDSSCs; with excitation of QDs electron and hole pairs are generated and electron is injected to mesoporous catalyst. Then transfer of electron occurs towards FTO surface and after that hole (which was generated with excitation of QD) would have oxidized the electrolyte. After reaching on FTO surface, electron flows towards counter electrode by external circuit and once electron was collected by counter electrode then it reduces the oxidized electrolyte.
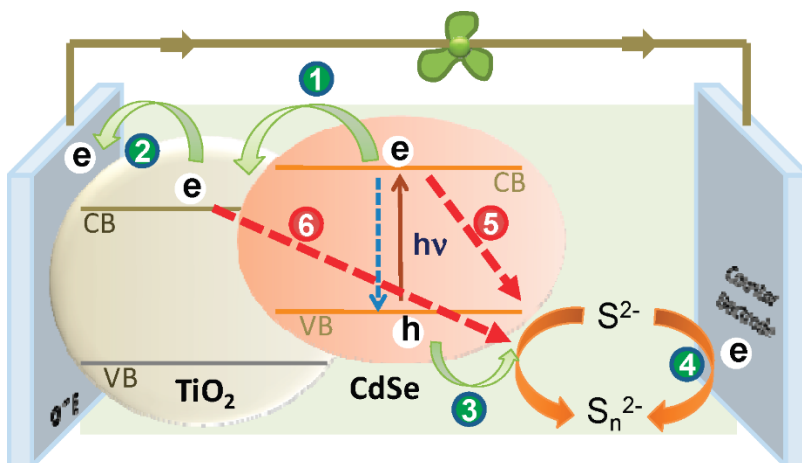
[Fig.9] Working principle of QDSSCs [21]

Chapter 2

Experimental section

2.1) Chemicals:

TiO$_2$ P25 powder, Titanium Chloride (TiCl$_4$), Triton X-100, Bismuth nitrate Bi(NO$_3$)$_3$, Sodium sulphide (Na$_2$S), Acetyl acetone, Deionized water, methanol, Acetone, Isopropanol, Ethanol, FTO (fluorine doped tin oxide glass) plates having resistance less than 30 $\Omega\ cm^{-2}$, Cu(NO$_3$)$_2$.3H$_2$O i.e. copper nitrate trihydrate, Sodium hydroxide, Ethylene diamine (C$_2$H$_8$N$_2$), Hydrazine hydrate (NH$_2$NH$_2$), tetrahydrofuran (THF).

2.2) Synthesis of Cu NPs:

In order to synthesize Cu NPs (shown in Fig.10), in a Teflon vessel first addition of 7 M NaOH (25 mL) followed by 0.1 M copper nitrate (0.15 mL), ethylene diamine (170 μL) which is used to control the size of NPs and hydrazine hydrate as reducing agent (30 μL). After adding all the reagents, the colour of solution was clear and used NaOH in excess for maintaining pH 14. This was heated into autoclave at 150 °C for 200 min. The copper NPs of Henna color were collected and stored in dark conditions. [19]
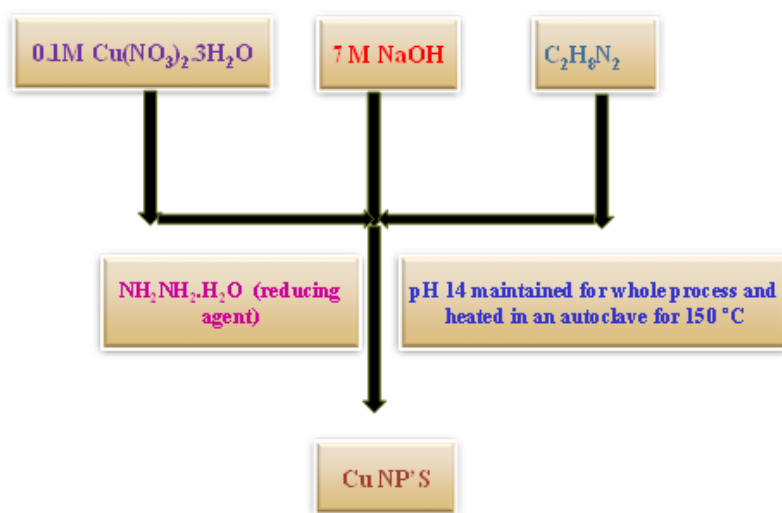

Fig.10 Synthesis of Cu NPs.

2.3) Fabrication of photoanode:

There are mostly deposition of three layers of TiO_2 mesoporous semiconductor and then deposition of QDs on photocatalyst. First layer: Active layer, Second layer: Scattering layer and Third layer: It is obtained by oxidation of aqueous $TiCl_4$ to increase the surface area and to improve QDs depositions.

Deposition of Active Layer:

Now for deposition of TiO_2 mesoporous semiconductor first paste is formed by TiO_2 P25 powder and by using solvent acetyl acetone 1.5 mL and 8.5mL Deionized water. And after sonication when the paste is completely uniform then addition of 20 mg of Triton X-100 followed by sonication. Then deposition of TiO_2 first layer on unmasked surface by doctor blading technique. Now after deposition of first layer on FTO plate the evaporation of solvents was done and settling the mesoporous particles followed by annealing at 500 °C for 30 min.

Deposition of Scattering layer:

After deposition of first layer the active area was again unmasked and same paste of TiO_2 P25 powder and solvent, Triton X-100 is pasted by doctor blading. And heating at 60 °C followed by annealing at 500 °C for 30 min.

Deposition of Third layer:

This layer is very thin layer as compared to above two deposited layers, main function of this layer to increase the active surface area and to improve QDs deposition. This layer is deposited by pouring the aqueous solution of $TiCl_4$ (0.04 M) on the electrodes and heating at 70 °C for 30 min. Then washing of the electrode with deionized water and again annealing at 500 °C for 30 min.

Deposition of Bi_2S_3 QDs:

So, mesoporous TiO_2 catalyst is prepared i.e. FTO/TiO_2. Now fabrication of Bi_2S_3 QDs on this surface was done by SILAR method. First cationic precursor i.e. Bi^{3+} was prepared by dissolution of 0.01 M of $Bi(NO_3)_3$ in acetone and anionic precursor was prepared by 0.01 M Na_2S in methanol. Now, FTO/TiO_2 plate was immersed in the solution of 0.01 M of bismuth nitrate and put for 10 s and after washing was put in oven at 60 °C for 2 min. Now, again FTO/TiO_2 plate was immersed in anionic precursor (0.01M solution of sodium sulphide in

methanol) solution and then rinsed with methanol, remove unabsorbed salts and dried at 60° C for 2 min. This was completion of 1 SILAR cycle shown in Fig.11 and deposition of 6 more SILAR cycles i.e. total 7 SILAR cycles of photoanode i.e. FTO/TiO$_2$/Bi$_2$S$_3$ of brown color electrode was obtained.
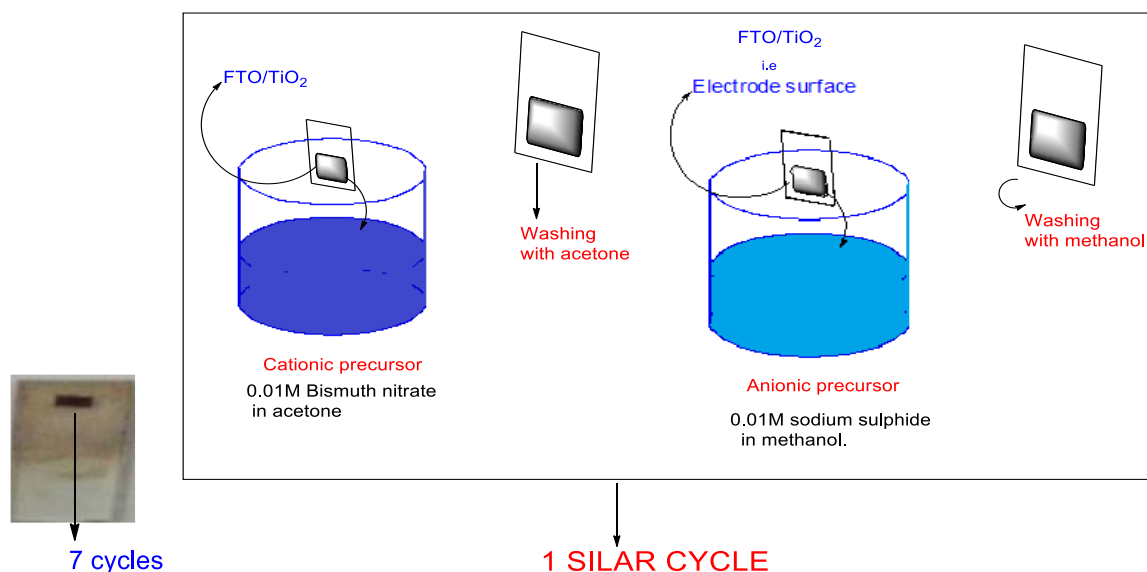
Fig. 11 Experimental setup of SILAR method of deposition of Bi$_2$S$_3$ QDs.

Deposition of Cu NPs on photoanode:

10 mg of synthesized copper nanoparticles were dissolved in 10 mL of deionised water and sonicated the mixture. Deposition of Cu NPs on TiO$_2$/Bi$_2$S$_3$ electrode was done by electrophoretic deposition method where TiO$_2$/Bi$_2$S$_3$ electrode was used as the working electrode and FTO as counter electrode. DC voltage of 15 V was applied for 5 min. Then Cu NPs were deposited on TiO$_2$/Bi$_2$S$_3$ electrode and dark green colour was obtained.

2.4) Electrolyte:

Electrolyte was used 0.1 M Na$_2$S in methanol/water of 7:3 (v/v) ratio. For all experiments same electrolyte was used.

2.5) Counter electrode for experiment:

A solution of 6 M H_2SO_4 and HNO_3 in 1:3(v/v) was formed and 0.2 g of MWCNTs were added to it followed by refluxation for 12 h at $80°C$. [22.] When the reaction mixture came at room temperature then the reaction mixture was diluted with deionized ultrapure water and was done till pH was 7. So, brown colored solid was collected and dispersed in water by sonication for 2 h. Then by EPD at 60 V a thin layer of functionalized MWCNTs was deposited over FTO/glass plate. After washing and evaporation of solvent used as counter electrode.

2.6) Spot-Shot Photos of photo-anode:
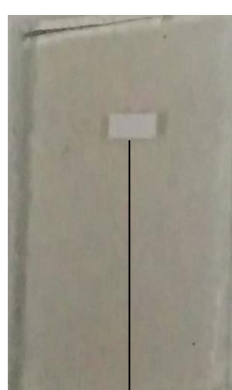
Three Layers of mesoporous semiconductor TiO_2

7 Layers deposited of Bi_2S_3 QDs on TiO_2 by SILAR.

Putting Cu NPs in neighbour to 7 Layers of Bi_2S_3 QDs on TiO_2.

Result and discussion

3.1 UV- Visible Spectroscopy Analysis:

The absorption spectra of Cu NPs, Bi_2S_3, TiO_2 and composite photoanode ($TiO_2/Bi_2S_3/Cu$) were recorded and shown in Fig.12. Fig.12 (a) shows absorption wavelength of Cu NPs was observed at 580 nm. Fig. 12 (b) Bi_2S_3 QDs shows absorbance at 740 nm (near infrared region). In Fig. 12 (c) TiO_2 absorbed in UV region at 380 nm. In Fig. 12(d) photoanode $TiO_2/Bi_2S_3/Cu$ shows absorption nearly in all region i.e. Cu NPs at 580 nm and Bi_2S_3 QDs shows at 740 nm and similarly TiO_2 shows at 380 nm. In the presence of Cu NPs, the photoanode ($TiO_2/Bi_2S_3/Cu$) shows strong absorption in the range of 350 -900 nm and it covers both visible and NIR regions.
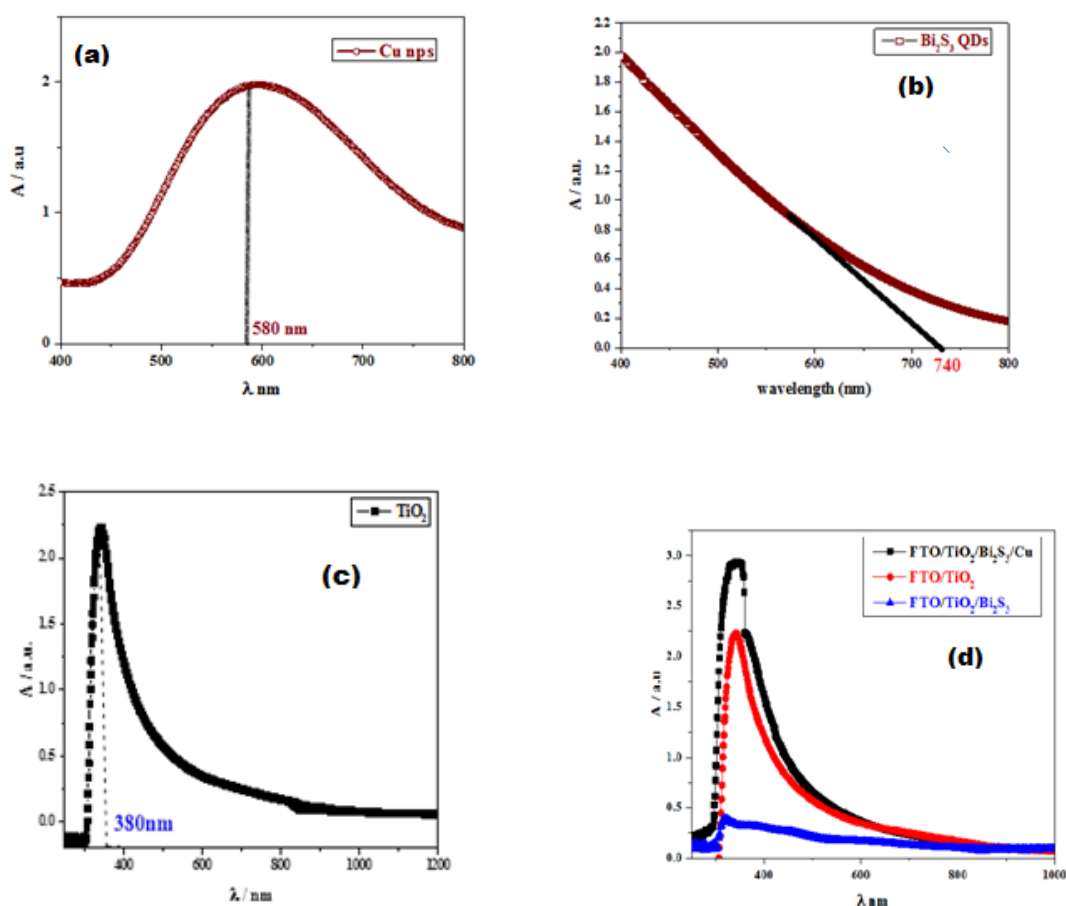

Fig. 12 UV-Visible spectra of (a) Cu NPs, (b) Bi_2S_3 QDs, (c) TiO_2 and (d) various photoanodes.

3.2 X-Ray Diffraction (XRD):

The crystal structure and lattice planes of TiO_2, Bi_2S_3 and Cu NPs are shown in figure (13). From XRD, the planes positions of TiO_2 are at (101), (103), (004), (200), (105), (211), (204), (116), (220), (215) and (224) [Fig.13 (b)] concurred with d = 3.51, 2.43, 2.36, 1.89, 1.69, 1.66, 1.47, 1.36, 1.33, 1.26 and 1.16 A^o respectively. Crystal system of TiO_2 is Tetragonal Body Centered Cubic lattice (JCPDS-894921). The planes of Bi_2S_3 are (110), (130), (211), (510) and (611) [Fig.13 (a)] with interplanar distances at d = 7.61, 3.56, 3.24, 1.69, 1.48 A^o respectively. The crystal system is orthorhombic with primitive lattice (JCPDS – 17-0320). The planes of Cu NPs are (111), (200), (220) and (311) [Fig.13(c)] with interplanar distances d = 2.08, 1.8, 1.5 and 1.27 A^o respectively and crystal system is Face Centered Cubic lattices. (JCPDS – 892838).
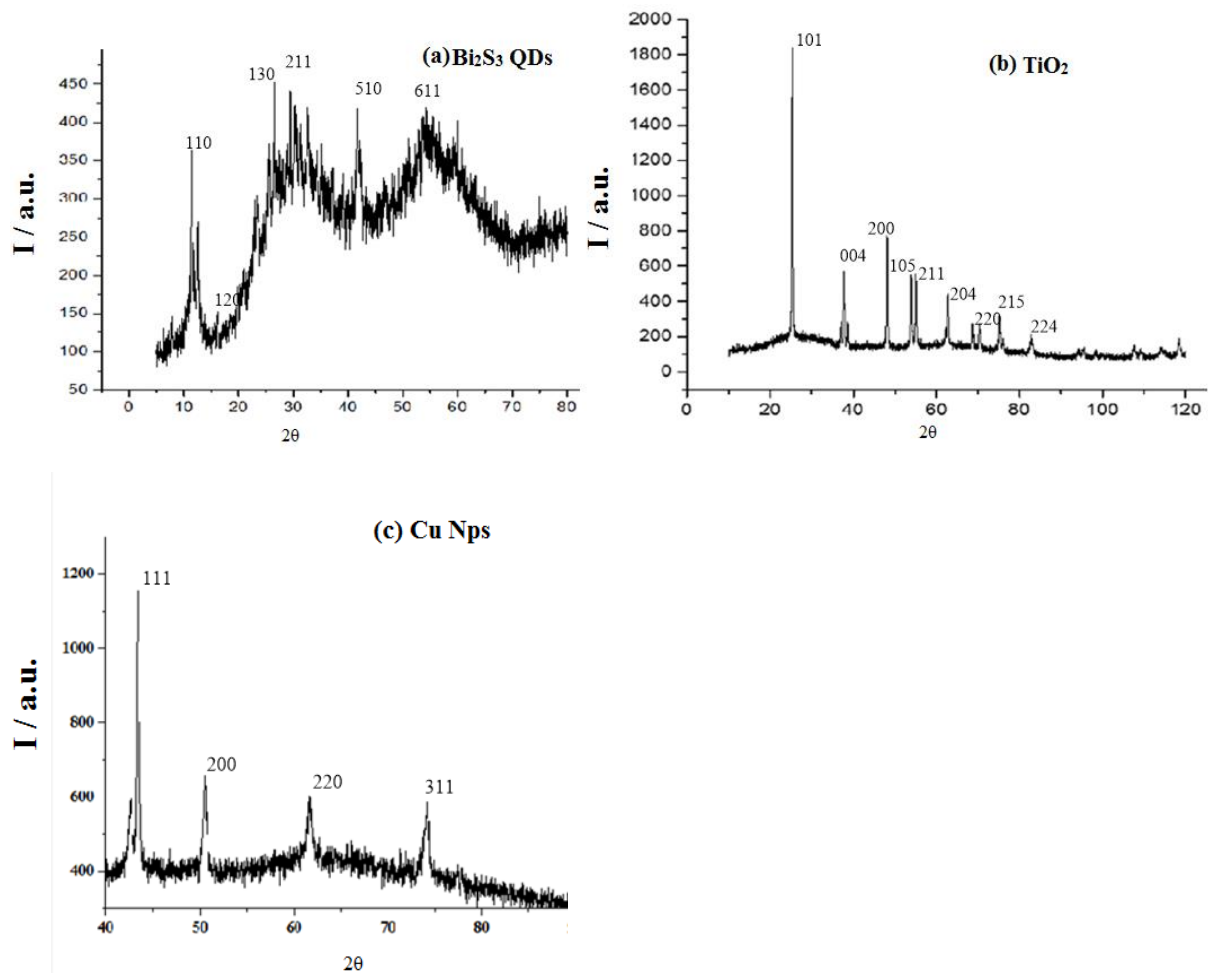

Fig. 13 XRD OF (a) Bi_2S_3 (b) TiO_2 and (c) Cu NPs.

3.3) Cyclic voltammetry analysis:

Cyclic voltammetry (CV) of TiO_2 and Bi_2S_3 films are shown in Fig.14. Herein, CV of TiO2 and Bi_2S_3 thin layer films were recorded in an aqueous 0.1 M KOH solution, which are working electrode & FTO plate as the counter electrode and Ag/AgCl/KCl was used as Reference electrode. Electrode potential of reference electrode is +0.197 V.

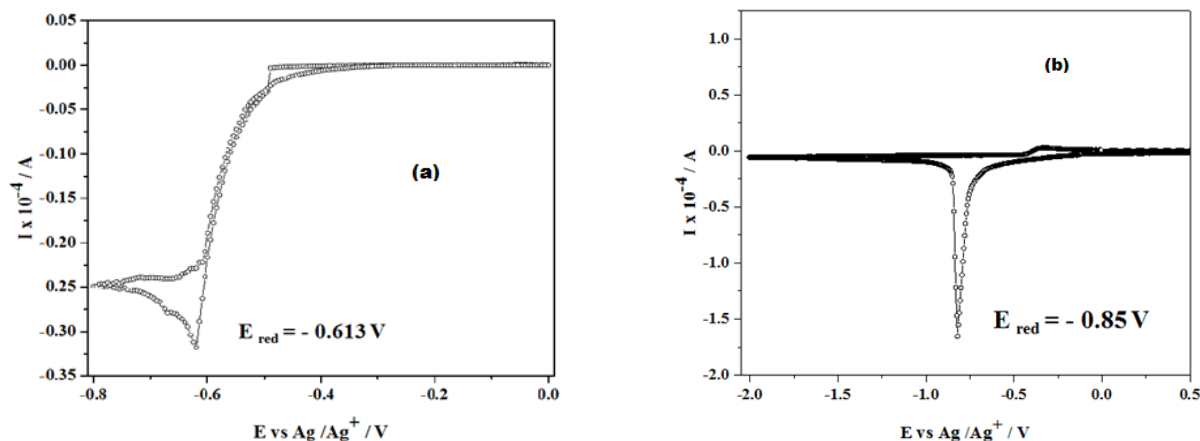**Calculation of CB and VB positions of TiO2 and Bi_2S_3:**

Fig.14 (a) CV of TiO2 and Fig.14 (b) CV of Bi2S3

Reduction potential of TiO2 was observed at -0.613V [Fig.14 (a)]

Electrode potential of reference electrode is +0.197 V.

Now, E_{red} relative to NHE is (- 0.613 V + 0.197 V) = - 0.416 V (NHE). A potential of 0 V (versus NHE) corresponds to 4.5 eV (w.r.t. vacuum level).

So, the position of CB in eV of TiO_2 is -4.084 eV. From UV-Visible spectroscopy the band gap of TiO_2 is 3.2eV. VB position of TiO_2 is (-4.084-3.2) eV = (-7.284 eV).

Similarly the CB and VB positions of Bi_2S_3 are found with the help of CV.

Reduction potential of Bi_2S_3 QDs is observed at -0.85 V [Fig.14 (b)]

E_{red} = - 0.85 V + 0.197 V = - 0.65 V (NHE).

E_{red} = -4.5 eV (0 V vs NHE) – (- 0.65 V) = - 3.84 eV. (CB)

Now, VB position is -3.84 eV + (- 1.67 eV) = - 5.51 eV.

3.4) J-V Curve:

Under an irradiance of 100 mA cm^{-2} Current density-Voltage (J-V) characteristics of the cells, were recorded and the counter electrode was MWCNTs/FTO. The power conversion efficiency (PCE) of devices (TiO_2/Bi_2S_3 and $TiO_2/Bi_2S_3/Cu$) were calculated with the help of J-V curve [Fig.15].
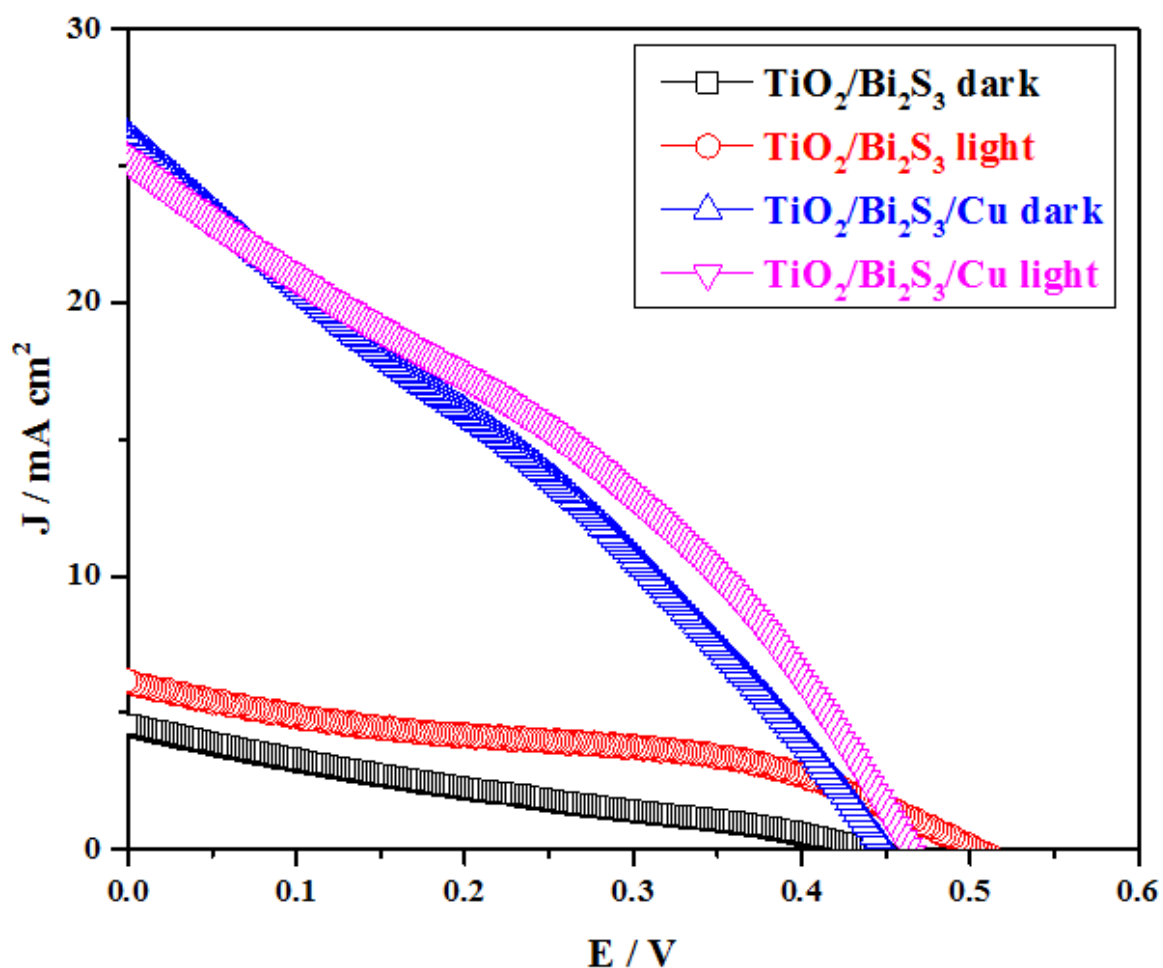

Fig. 15 J-V curve of experimentally prepared devices.

Due to thermoelectric behaviour of Bi_2S_3, dark current may be produced and hence efficiency. The highest efficiency of TiO_2/Bi_2S_3 devices are 0.516 and 1.202 in dark and light respectively. (Table 1) shows PCE improvement in photoanode when Cu NPs deposited on Bi_2S_3 QDs.

Photo anode configuration	V_{oc}(V)	J_{sc}(mA/cm^2)	FF	$\eta\%$
TiO$_2$/Bi$_2$S$_3$ dark	0.435	5.08	0.23	0.516
TiO$_2$/Bi$_2$S$_3$ Light	0.501	6.12	0.39	1.202
TiO$_2$/Bi$_2$S$_3$/Cu dark	0.448	26.02	0.29	3.407
TiO$_2$/Bi$_2$S$_3$/Cu light	0.462	25.12	0.33	3.902

Table 1 J-V characteristics of TiO$_2$/Bi$_2$S$_3$ and TiO$_2$/Bi$_2$S$_3$/Cu electrodes.

3.5) Impedance analysis:

The fitted parameters [Fig. 16] gives the valuable information as from following parameters: R_1 is the bulk resistance of the 0.1 M Na$_2$S solution; R_2 is the resistance offered to charge transfer at the photoanode /electrolyte interface and R_3 is the differential resistance offered by the solution to movement of redox species in the electrolyte. Y_0 (1) represents the ease with which charge can flow and Y_o (2) is the measure of differential conductance for the electrolyte.
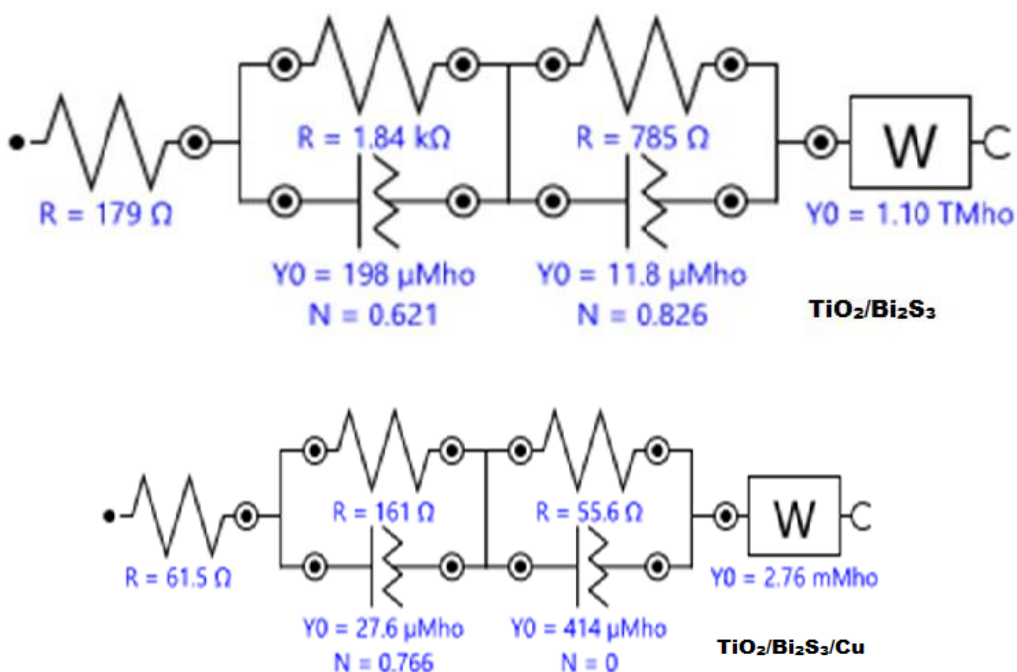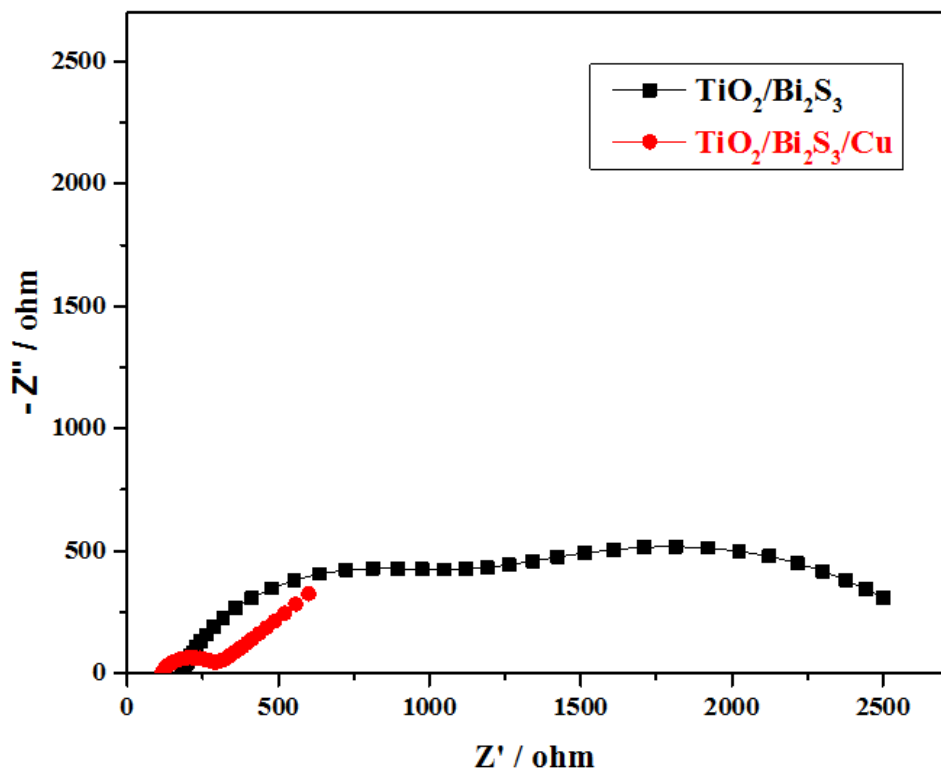
Fig. 16 Impedance study TiO_2/Bi_2S_3 and $TiO_2/Bi_2S_3/Cu$ devices.

S.No.	Device	R_1 Ω	R_2 Ω	R_3 Ω	Y0(1) (µMho)	Y0(2) (µMho)	N_1	N_2	W
1	TiO$_2$/Bi$_2$S$_3$	179 Ω	1.84(KΩ)	785Ω	198	11.8	0.621	0.826	1.10(TMho)
2	TiO$_2$/Bi$_2$S$_3$/Cu	61.5Ω	161 Ω	55.6Ω	27.6	414	0.766	0	2.76(mMho)

Table 2 Impedance data of TiO$_2$/Bi$_2$S$_3$ and TiO$_2$/Bi$_2$S$_3$/Cu electrodes.

From Table 2 data, it can be conclude that R$_1$, R$_2$ and R$_3$ of device TiO$_2$/Bi$_2$S$_3$/Cu are lesser than that of TiO$_2$/Bi$_2$S$_3$ devices.

3.6) Energy-Level positions of the device:

From CV we found CB positions and by UV-Visible spectra band gap of TiO$_2$ and Bi$_2$S$_3$.
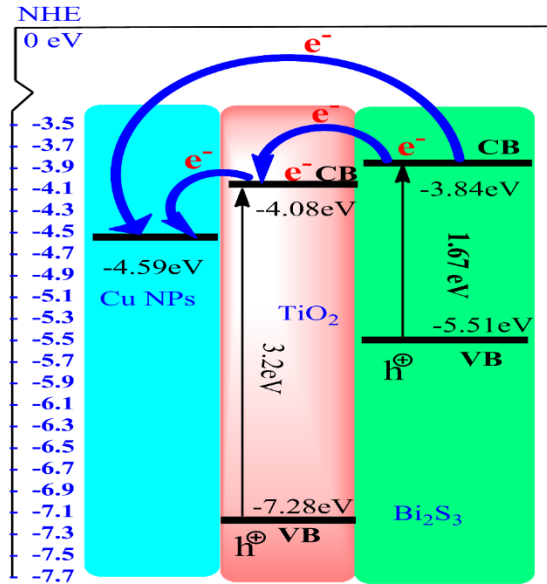

Fig. 17 Electron flow of TiO$_2$/Bi$_2$S$_3$ /Cu device.

Fig. 17 represents the energy-level diagram of electron flow of TiO$_2$/Bi$_2$S$_3$ /Cu photoanode. The ultimate electron collector are Cu NPs as shown.

Conclusions:

Titanium dioxide/bismuth sulphide (TiO_2/Bi_2S_3) and Titanium dioxide/bismuth sulphide/Copper nanoparticles (TiO_2/Bi_2S_3/Cu) devices are successfully formed and deposition of Bi_2S_3 on mesoporous photo-catalyst was done by SILAR process and then deposition of Cu NPs was done by Electrophoretic deposition method. Probably due to thermoelectric behaviour of Bi_2S_3, considerable efficiency in the dark efficiencies were observed. TiO_2/Bi_2S_3 devices showed the efficiency of 0.516 and 1.202 in dark and light, respectively. On depositing Cu NPs on Bi_2S_3 QDs, the performance of devices increased to 3.40 % and 3.90 % in dark and light respectively.

References:

[1]. Williams, R. Becquerel photovoltaic effect in binary compounds. J. Chem. Phys. **1960**, *32*, 1505–1514.

[2.] Chapin, D. M., Fuller, C. S., & Pearson, G. L. A new silicon p-n junction photocell for converting solar radiation into electrical power. J. Appl. Phys. **1954**, *25(5)*, 676-677.

[3.] "Solar photovoltaic cells." J. Chem. Educ. **1981**, *58, no. 5* 418.

[4.] Lee, Hsin-Cheng and Wu, Shich-Chuan and Yang, Tien-Chung and Yen, Ta-Jen; Efficiently harvesting sun light for silicon solar cells through advanced optical couplers and a radial pn junction structure, Energies **2010**, *3 no.4*, 784--802

[5.] Kim, M. R., & Ma, D. Quantum-dot-based solar cells: recent advances, strategies, and challenges. J. Phys. Chem. Lett. **2014**, *6*(1), 85-99.

[6.] Lee, M. M., Teuscher, J., Miyasaka, T., Murakami, T. N., & Snaith, H. J. Efficient hybrid solar cells based on meso-superstructured organometal halide perovskites. Science **2012**, *338*(6107), 643-647.

[7.] Liao, S. H., Jhuo, H. J., Yeh, P. N., Cheng, Y. S., Li, Y. L., Lee, Y. H., ... & Chen, S. A. Single junction inverted polymer solar cell reaching power conversion efficiency 10.31% by employing dual-doped zinc oxide nano-film as cathode interlayer. Scientific reports **2014**, *4*.

[8.] Zaban, A. M. O. I., Micic, O. I., Gregg, B. A., & Nozik, A. J. Photosensitization of nanoporous TiO_2 electrodes with InP quantum dots. Langmuir **1998,** *14*(12), 3153-3156.

[9.] Chuang, C. H. M., Brown, P. R., Bulović, V., & Bawendi, M. G. Improved performance and stability in quantum dot solar cells through band alignment engineering. Nature materials **2014** *13*(8), 796.

[10.] Alivisatos, A. P. Semiconductor clusters, nanocrystals, and quantum dots. Science **1996**, *271*(5251), 933.

[11.] Boercker, J. E., Clifton, E. M., Tischler, J. G., Foos, E. E., Zega, T. J., Twigg, M. E., & Stroud, R. M. Size and temperature dependence of band-edge excitons in PbSe nanowires. J. Phys. Chem. Lett. **2011**, *2*(6), 527-531.

[12.] Yu, W. W., Qu, L., Guo, W., & Peng, X. Experimental determination of the extinction coefficient of CdTe, CdSe, and CdS nanocrystals. Chem. Mater. **2003**, *15*(14), 2854-2860.

[13.] Nozik, A. J. Quantum dot solar cells. Physica E (Low-dimensional Systems and Nanostructures) **2002**, *14(1)*, 115-120.

[14.] Nozik, A. J. Multiple exciton generation in semiconductor quantum dots. Chem. Phys. Lett. **2008**, *457*(1), 3-11.

[15.] Desai, J. D., & Lokhande, C. D. Chemical deposition of Bi_2S_3 thin films from thioacetamide bath. Mater. Chem. Phys. **1995**, *41*(2), 98-103.

[16.] Kelly, K. L., Coronado, E., Zhao, L. L., & Schatz, G. C. The optical properties of metal nanoparticles: the influence of size, shape, and dielectric environment. J. Phys. Chem. B **2003** *107*(3), 668-677.

[17.] Yun, J., Hwang, S. H., & Jang, J. Fabrication of Au@ Ag Core/Shell Nanoparticles Decorated TiO2 Hollow Structure for Efficient Light-Harvesting in Dye-Sensitized Solar Cells. ACS Appl. Mater. Interfaces **2015**, *7*(3), 2055-2063.

[18.] Zhou, N., López-Puente, V., Wang, Q., Polavarapu, L., Pastoriza-Santos, I., & Xu, Q. H. Plasmon-enhanced light harvesting: applications in enhanced photocatalysis, photodynamic therapy and photovoltaics. RSC Adv. **2015**, *5*(37), 29076-29097.

[19.] Kumar, P. N., Deepa, M., & Ghosal, P. Low-Cost Copper Nanostructures Impart High Efficiencies to Quantum Dot Solar Cells. ACS Appl. Mater. Interfaces **2015**, *7*(24), 13303-13313.

[20.] Kamat, P. V., Tvrdy, K., Baker, D. R., & Radich, J. G. Beyond photovoltaics: semiconductor nanoarchitectures for liquid-junction solar cells. Chem. Rev. **2010**, 110(11), 6664-6688.

[21.] Kamat, P. V. Boosting the efficiency of quantum dot sensitized solar cells through modulation of interfacial charge transfer. Acc. Chem. Res. **2012,** *45,* 1906-1915.

[22.] Kumar, P. N., Mandal, S., Deepa, M., Srivastava, A. K., & Joshi, A. G. Functionalized graphite platelets and lead sulfide quantum dots enhance solar conversion capability of a titanium dioxide/cadmium sulfide assembly. J. Phys. Chem. C **2014**, *118*(33), 18924-18937.